Research Article

Check for updates

Ce-doped Nanobioactive Glass/ Collagen/ Chitosan Composite Scaffolds: Biocompatibility with Normal Rabbit's Osteoblast Cells and Anticancer Activity Test

HANAN FATHY HAMMOUDA[1], MOHAMMAD MAHMOUD FARAG[2*], MERVET M.F. EL DEFTAR[3], MOHAMED ABDEL-GABBAR[4], BASANT M. MOHAMED[4]

[1]The Healthy Chemistry Department, Center Public Health Laboratory, Ministry of Health, Egypt; [2]Glass Research Department, National Research Centre, Dokki, 12622, Giza, Egypt; [3]Department Pathology, Tissue Culture and Cytogenesis Unit, National Cancer Institute, Cairo University, Egypt; [4]Department of biochemistry, Faculty of Science, Beni-Suef University, Beni-Suef, Egypt.

Abstract | This research aims to evaluate cerium-doped nanobioactive glass/collagen/chitosan composites scaffolds with osteoblast mineralization of normal rabbit bone marrow mesenchymal stem cells (rBM-MSCs) and cancer osteosarcoma cells. The non-cellular *in vitro* bioactivity test was performed in simulated body fluids for periods 1, 3, 10, 20 and 30 d by measuring the calcium and phosphate ion concentrations by SEM/EDX analysis. While, the bioactivity of expanded and differentiated osteoblast cells derived from isolated rBM-MSCs by flowcytometric analysis was studied by histochemical staining with Alizarin Red and von Kossa to confirm the osteogenic differentiation process. Also, cell viability assay by MTT was used to measure the number of viable osteoblast cells cultured with scaffolds extracts. Also, the antitumor activity of the scaffolds was studied against cancer osteosarcoma cell lines using Sulforhodamine B (SRB) assay. The results showed that addition of cerium-doped nanobioactive glass to the composite scaffolds was triggered an increase in cell growth, proliferation and mineralization markers of osteoblast cells that increased with time as the highest concentrations of CeO_2 in nanobioactive glass (sample CL/CH/C10). Cell viability proved also that all scaffolds and their extracts showed proliferation inhibition with time < 25% reference to final cell number of control cells. Among the composites, having CL/CH/C5 showed the highest cytotoxic effect and reduced survival rate of osteosarcoma cells to 75.68% after 24 h. The subsequent increase of CeO_2 concentration was also effective but its effect was less than CL/CH/C5 sample. Finally, cerium-doped nanobioactive glass/collagen/chitosan composites scaffolds were exhibited good biocompatibility on normal cells and increased cytotoxicity on cancer osteosaroma cells.

Keywords | Bioactivity, Scaffold, Osteogensis, Cerium oxide particles, Mesenchmal stem cells, Osteosarcoma cells

INTRODUCTION

Research for new multifunctional scaffolds for tissue engineering applications is a critical and important issue in the biomedical field. The Ideal scaffold should be characterized by good biocompatiblity, interconnected porous structure, and desirable mechanical properties (Lehmann et al., 2010). The scaffolds based on natural polymers (like collagen, chitosan, and gelatin) are favored compared to the synthetic polymers. Collagen is the richest protein in the extracellular matrix, and the cellular attachment binding is achieved by it causing rising of cell growth and proliferation (Gordon et al., 2004; Ignatius et al., 2005). Chitosan possesses good biodegradability, cell compatibility, haemostatic activity, mucoadhesion, and limited immunogenicity (Lahiji et al., 2000; Rinaudo, 2006). These unique properties of both polymers make them to be widely used in tissue engineering applications,

and fabrication of composite scaffolds based on these two polymers permits to obtain scaffolds with superior characteristics (Arpornmaeklong et al., 2021; Suo et al., 2021; Yang et al., 2021).

Despite the advantages of collagen and chitosan scaffolds in the tissue engineering the main drawback is their biological inertness aspect. Accordingly, bioactive fillers (such as, bioactive glass) have been suggested to be incorporated in this kind of polymers to improve their bioactivity (Kaczmarek et al., 2020; Gao et al., 2021; Deen et al., 2022). Moreover, the scaffold can be functionalized with by doping of bioactive glass filler with therapeutic ions such as, silver, copper and cerium, in these fillers.

Cerium compounds (such as, cerium (III) oxalate, cerium (III) iodide, and cerium nitrate) have been used in biomedical application to treat many types of diseases (Xu and Qu, 2014) and several symptoms (Maccarone et al., 2020; Abbasi et al., 2021; Asgharzadeh et al., 2021; Sundararajan et al., 2021). These various biomedical effects related to its properties, such as a resemblance to calcium, antibacterial and immunomodulatory properties. In addition, cerium when merged with oxygen in a nanoparticle formulation gains fluorite crystalline structure with unique properties like excellent catalytic activities and multienzyme-mimetic properties; including superoxide oxidase, catalase and oxidase, mimetic properties which are derived from quick and proper transformation of the oxidation state between Ce^{4+} (fully reduced) and Ce^{3+} (fully oxidized). All these properties protrude it as a charming and gainful material with dual role as an oxidation catalyst and reduction catalyst, depending on the reaction conditions. This increased its use widely in high-technology industries such as information, biotechnology; drug delivery devices and bio-scaffold and other applications in biological fields (Corma et al., 2004; Karakoti et al., 2010; Mandoli et al., 2010; Bouzigues et al., 2011; Celardo et al., 2011; Li et al., 2013; Xu et al., 2013). Moreover, recent *in vitro* studies have been shown that cerium oxide nanoparticles are cytotoxic to cancer cells, inducing oxidative stress and induced apoptosis to cancer cells by several mechanisms lipid damage, protein and DNA inverse to normal cells (Lin et al., 2006). It protects it from ROS damage (Perez et al. 2008). Therefore, doping of bioactive glass with cerium ion can be useful for cancer treatment, and so, cerium has been incorporated in the bioactive glasses in previous studies (Leonelli et al., 2003; Zhang et al., 2010; Du et al., 2011; Shruti et al., 2012; Goh et al., 2014; Deliormanlı, 2015; Gupta et al., 2016; Nicolini et al., 2016, 2017; Placek et al., 2018; Farag et al., 2019; Abbasi et al., 2021).

Cytotoxicity test became an important step towards the animals testing and finally clinical trials that will determine the biocompatibility of the material in a given application.

Sulforhodamine B (SRB) method (Skehan et al., 1990; Vichai and Kirtikara, 2006; Orellana and Kasinski, 2016); a rapid, sensitive colorimetric and reproducible method for measuring the agent cytotoxicity in both attached and suspension cell cultures. It provided good linearity with cell number, is less sensitive to environmental metabolism, and provided a fixed end point that is not require a time sensitive measurement of initial reaction velocity. It is used to evaluate colony formation and colony deactivation (Orellana and Kasinski, 2016).

This work was aimed to evaluate the effect of Ce-doped nanobioactive glass filler in collagen/chitosan scaffolds on the biocompatibility and to study deeply the in vitro bioactivity test of osteoblast cells derived from bone marrow mesenchymal stem cells (BM-MSCs) for three weeks of differentiation and characterized that with specific markers of osteogensis process. According to our knowledge, there have no much data about bioactivity of composite scaffolds based on collagen and chitosan polymer blend used as a polymer matrix for nanobioactive glass doped with different ratios of CeO_2. The cellular in vitro biocompatibility test was performed by direct contact of the osteoblast cells with different fabricated nanocomposite scaffolds and by indirect test using the fluid extracts of these scaffolds to the cells. Also, we evaluated the antitumor activity the scaffolds using MG-63: Osteosarcoma.

MATERIALS AND METHODS

MATERIALS

TEOS (tetraethyl ortho silicate), boron alkoxide, $Ca(NO_3)_2 \cdot 4H_2O$, TEP (triyethyl phosphate), $Ce(NH_4)_2(NO_3)_6$ (ammonium cerium (IV) nitrate, ethanol (EtOH), collagen, chitosan. Two different culture media were prepared to enhance both cellular proliferation in primary culture and osteogenic differentiation. The media was consisted mainly of DMEM, nutrient mixture Ham's F12, 10 % FBS, 1% L- glutamine, 1% penicillin-streptomycin (100 U/ml-100 µg/ ml), and 1 ng b-FGF for primary culture with addition of 50 µM L-ascorbic acid 2-phosphate, 100 nM dexamethasone, and 1 mM β- glycerophosphate for osteogenesis processes.

PREPARATION OF COMPOSITE SCAFFOLDS

Different composite scaffolds based on collagen, chitosan and/or nano-bioactive glass (nBG) were prepared by thermal-induced phase separation method, with 1:1 volume ratio collagen and chitosan, as a polymer matrix, and the glass was added to the scaffold with 30 wt.%. The glasses were prepared based on (80-x) SiO_2-15CaO-$5P_2O_5$-xCe_2O, in mole % (x= 0, 5 and 10 mole %), accordingly, the glass encoded as BG-C0, BG-C5 and BG-C10, respectively, by a quick alkali-mediated sol-gel

method (Xia and Chang, 2007), and the derived scaffolds were named as; scaffolds encoded as CL/CH, CL/CH/C0, CL/CH/C5 and CL/CH/C10, where CL/CH did not contain glass particles. The microstructure and morphology of the scaffolds were characterized by scanning electron microscope coupled with dispersive x-ray analysis, SEM/EDX (model, HITATCHI Su800).

EVALUATION OF SCAFFOLDS BIOACTIVITY
NON-CELLULAR BIOACTIVITY TEST
The non-cellular in vitro bioactivity test was performed in the simulated body fluid (SBF), prepared according to (Kokubo and Takadama, 2006), to track the formation of bone-like apatite on the surface of composite scaffolds throughout the soaking time. Different scaffolds were put into a vessel containing SBF and placed in the incubator at 37°C for periods 1, 3, 10, 20 and 30 d. At the predetermined periods, the pH, weight loss (%) and water uptake (%) were measured. as well as, the calcium and phosphate ion concentrations released from the scaffolds into SBF were measured by measured using the colorimetric kits (SPECTRUM, Egypt) or ICP (inductively coupled plasma). The weight loss (%) was calculated using Equation 1, and the water uptake percentage was calculated according to Equation 2.

$$\text{Wt. loss \%} = (W_i - W_d/W_i) \times 100 \quad …(1)$$
$$\text{Water uptake \%} = (W_w - W_i/W_i) \times 100 \quad …(2)$$

Where; W_i, W_d and W_w are the initial weight, weight after soaking in SBF and dried, and weight of the scaffold saturated with water, respectively. Additionally, the scaffold surfaces were characterized by the scanning electron microscope coupled with energy dispersive X-ray analysis (SEM/EDX), to investigate the hydroxyapatite layer formed on the scaffold samples.

CELL VIABILITY TEST
In this study, bone marrow mesenchymal stem cells (BM-MSCs) were utilized for cell viability test of the scaffolds. The cells were isolated from the femurs and tibia of six rabbits, 2 to 3 months old. The rabbits were scarified by cervical dislocation in the animal house lab using the guidelines approved by the Institutional Animal Care and Use Committee, Beni-Suef University (BSU-IACUC), and the approval number is 021-194, and their thighs were isolated then swabbed with 70% alcohol. The femur and tibia bones were removed keeping their heads intact. The bones were transferred immediately in 70% alcohol to the tissue culture lab.

Inside the biological safety cabinet, the bones were cleaned of adherent soft tissue. The epiphyses were removed using sterile tweezers and scissors. The marrow was then flushed out from tibia and femur bones using a 5-ml syringe

containing growth medium. The resulting cell suspension was centrifuged for 5 min at 1000 rpm.

CULTURING AND EXPANSION OF BM-MSCs
Cells were collected and re-suspended in 1 ml growth medium then counted and seeded at concentration of 1 x 10^5 cells/ ml in a T25 flask for 3 d using complete expansion medium supplemented with 1ng/ml b-FGF. Non adherent cells were removed, and then the medium was routinely changed every 3 d. The inverted phase contrast microscope was used to examine the cells daily through primary culture. When culture cells reached 80% confluence, the cells were washed twice with D-PBS and the cells were tryps inized with 0.25% trypsin. Cell counting and viability were assessed by trypan blue exclusion using Countess Automated Cell Counter (Invitrogen).

CHARACTERIZATION OF IMMUNOPHENOTYPE
For flow cytometric analysis, A total 100,000 to 200,000 cells were incubated at 4 °C for 20 min in the dark with the following isotype; CD34 (hemopoietic stem cell marker) as a negative marker and CD73, CD90, CD146 and CD105 (panel specific for human multi potent mesenchymal stromal cells as a positive marker, Multicolor flow cytometry kit Cat. No: FMC002). Flow cytometry was performed using forward scatter and side scatter analysis to gate for live cells. Use isotype controls to set photo-multiplier tube (PMT), compensation, and analysis gates.

INDUCTION OF OSTEOGENESIS DIFFERENTIATION OF BM-MSCs
For osteogenic induction of the rabbit BM-isolated spindle-shaped fibroblastic-like cells, a protocol described by Jaiswal was used (Jaiswal et al., 1997). Subculture cells were seeded in 24-well plate at a density of 5000 cells/ cm² in osteogenic medium. Subculture was maintained in a humidified atmosphere of 5% CO_2 at 37°C for 21 d. The medium was changed every 3-4 d and subculture was performed before cells reached confluence. As a negative control some cells were maintained in complete expansion medium lacking osteogenic factors, in parallel to osteogenic differentiation experiment. Osteogenesis markers were assayed at weekly intervals for three weeks at 7, 14 and 21 d of osteogenic differentiation (Declercq et al., 2004).

ALKALINE PHOSPHATASE (ALP) ACTIVITY ASSAYS
ALP activity of BM-MSCs was assessed by biochemical and cytochemical assays (Ng et al., 2008; Augello and De Bari 2010). In the biochemical assay *p*-nitrophenyl phosphate (pNPP) was used as a phosphatase substrate. Cells were harvested by trypsinization and lysed with 0.5% Triton X-100. The cell lysates were then mixed with pNPP substrate solution (Tris–glycine buffer pH 10.3, $MgCl_2$

and p-nitrophenyl phosphate) and incubated at 37°C for 30 min. The reaction was stopped by the addition of 3 M NaOH and the amount of p-nitrophenol released was measured at wavelength 405 nm in a micro-plate reader. The *p*-nitrophenol quantity liberated was determined using a curve generated from known concentrations of *p*-nitrophenol standards. All values were normalized against the cell number. For cytochemical ALP staining, cells were washed with PBS, dried, and fixed in ice cold methanol at room temperature for 30 seconds. Fixed cells were stained by Fast Violet B salt and Naphthol AS-MX phosphate for 10 min and then counterstained in sufranin for 5 min.

Matrix mineralization assays

The extracellular matrix mineralization was determined by measuring Ca deposits for bone nodule formation. The cellular matrix was stained using Alizarin red S dye (sodium alizarin sulphonate) staining which combines with Ca in the matrix. Because Ca co-precipitates with the phosphate ion in the matrix, von Kossa staining (which stains phosphate ions) was also used for the determination of mineralized nodules. The conditions of sub-cultured cell scaffolds and sub-cultured cell scaffolds extract for staining were the same as those described on cell culture. The fixed scaffolds in tissue culture wells with paraformaldhyde were then examined with microscopy using inverted phase-contrast microscope with a digital camera Olympus at day 14 and day 21 (Hale et al., 2000; Rao et al., 2001).

MTT assay

Survivals rate of the composite scaffolds and their extracts with cells was examined daily under an inverted light microscope for cell morphology. Besides, number of seeded culture plates of four composite scaffold/cells and its extracts was washed in PBS, cells counting and viability were determined by MTT assay (Kamal et al., 2013).

Antitumor activity

MG-63: Osteosarcoma was obtained from Nawah Scientific Inc., (Mokatam, Cairo, Egypt). Cells were thawed and propagated for three passages in DMEM supplemented with 100 mg/mL of streptomycin, 100 units/mL of penicillin and 10% of heat-inactivated fetal bovine serum in flasks of 25 and 75 cm² surfaces in humidified, 5% (v/v) CO_2 atmosphere at 37 °C.

The cell viability test was assessed by SRB assay (Skehan et al., 1990). Aliquots of 100 μL cell suspension ($5x10^3$ cells) were in 96-well plates and incubated in complete media for 24 h. before cell seeding, all composite materials discs were sterilized with gamma rays. After sterilization, the scaffolds discs were pre-soaked in DMEM for 12h. Subsequently, discs were incubated with cells for 1h and 24h at 37°C in 5%

CO_2 incubator. After 1 hand 24 h of materials exposure, all discs were rinsed with PBS to remove non- adhering cells. Cells were fixed by replacing media with 150 μL of 10% TCA and incubated at 4 °C for 1 h. The TCA solution was removed, and the cells were washed 5 times with distilled water. Aliquots of 70 μL SRB solution (0.4% w/v) were added and incubated in a dark place at room temperature for 10 min. Plates were washed 3 times with 1% acetic acid and allowed to air-dry overnight. Then, 150 μL of TRIS (10 mM) was added to dissolve protein-bound SRB stain; the absorbance was measured at 540 nm using a BMG LABTECH®- FLUOstar Omega microplate reader (Ortenberg, Germany). Also, cytotoxicity was examined under an inverted light microscope after 1h and 24h of incubation. Triplicates well were used for each sample.

Statistical analysis

Where indicated, experimental data are reported as mean ± SD of triplicate or more independent samples. Statistical analysis was performed using Microsoft® Office Excel 2010 software. Significant differences were detected by the students *t*-test. The probability level (P) at which differences were considered significant was $P < 0.05$ versus control.

RESULTS AND DISCUSSION

In vitro bioactivity

The *in vitro* bioactivity test in SBF is considered an important preliminary test in the evaluation of biocompatibility of tissue engineering scaffolds. Where, the ability of the scaffold to form a bone-like apatite layer on its surface after immersion in SBF is reflected the capacity of material to connect with the human bone living cells. Figure 1 presents the SEM photos coupled with EDX analysis of the surface of CL/CH, CL/CH/C0, CL/CH/C5 and CL/CH/C10 scaffolds after soaking in SBF for 30d. The SEM micrograph was showed that there was no bone-like apatite layer observed on the collagen/chitosan scaffold (CL/CH sample), and there was no peaks corresponding to Ca and P atoms were detected by EDX analysis. Whereas, the apatite crystals were observed on the scaffolds contained NBG particles which confirmed by the EDX spectra. Where, the Ca and P atomic weight percentage became relatively higher than that of Si.

The variation in pH of SBF contained CL/CH, CL/CH/C0, CL/CH/C5 and CL/CH/C10 was tracked at predetermined times. Figure 2A shows the pH change of SBF as a function of time during soaking in SBF up to 30 d. It can be observed from the figure that the variation of pH of SBF incubated all samples were similar. Where, the pH was increased from 7.40 to about 7.53, 7.54, 7.54, and 7.60 after 3d followed by continuous increase to reach maximum

values at day 10 of soaking to become 7.80, 7.82, 7.81, and 7.87 for CL/CH, CL/CH/C0, CL/CH/C5 and CL/CH/C10, respectively. The pH was decreased progressively up to the end of immersion time. In addition, Figure 2B represents the weight loss % of different scaffolds. The weight loss profiles for all scaffolds were similar. Where, it slightly increased up to 20 d of incubation, followed by abrupt increase till the end of soaking time which can be described by burst degradation. The weight loss % became 51.8% 62.3%, 49.9%, and 42.2%. On the other hand, the weight loss % of CL/CH scaffold was significantly (p < 0.015) less than that of other scaffolds during 20 d of soaking, but difference became insignificant after this time.
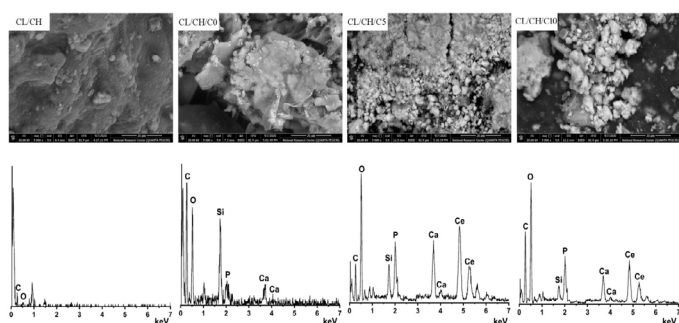

Figure 1: SEM and EDX of CL/CH, CL/CH/C0, CL/CH/C5 and CL/CH/C10 samples after immersion in SBF for 30 d.
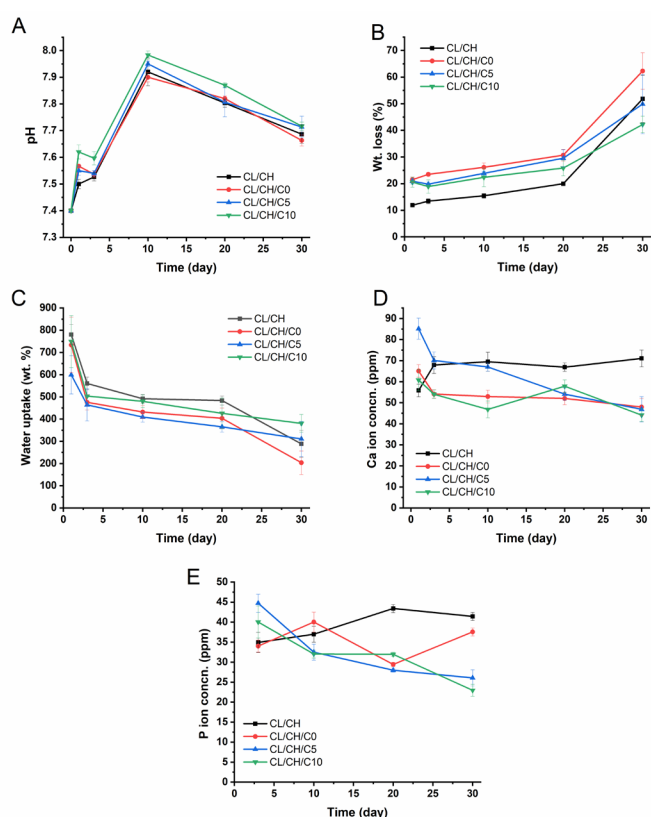

Figure 2: (A) pH, (B) weight loss (%), (C) water uptake (wt. %) (D) Ca^{2+} ion concentration (ppm), (E) phosphate ion concentration (ppm) of CL/CH, CL/CH/C0, CL/CH/C5 and CL/CH/C10 samples.

The water uptake measurement of the scaffold materials is important for the cell adhesion on the scaffold surface, where, the wetting of surface affects the initial protein attachment which is potentially useful for the cell attachment and proliferation (Arima and Iwata, 2007). Figure 2C presents the water uptake % of CL/CH, CL/CH/C0, CL/CH/C5, and CL/CH/C10. As shown from the figure, the water uptake was initially increased to 780.4 %, 733.8 %, 599.2 %, and 749.1 % for CL/CH, CL/CH/C0, CL/CH/C5, and CL/CH/C10, respectively, while it decreased throughout the immersion time due to the scaffold degradation.

The concentration variations of Ce, Ca, and P ions in SBF were also measured as a mark of bone-like apatite formation on the scaffold surfaces. Figure 2D and E show the concentration of Ca and P ions only; because of Ce ion concentration in the solution was too small to be detected (< 1 ppm). The Ca and P ion concentrations were decreased with the time or the scaffolds contained NBG particles, while, the concentration was nearly constant for the solution incubated collage/chitosan scaffold. That was due to nearly a lack of reaction between the polymer and the SBF. The decrease of Ca and P ion concentrations through the soaking time can be assigned to a spending of such ions in the formation of bone-like apatite layer on the scaffold contained NBG particles.

Cell viability
Isolation, expansion, osteogenic differentiation and mineralization assays primary culture, and first passage of (rabbit BM-MSCs) in expansion medium

Following BM-MSCs deposition in expansion medium (Figure 3A and B), all rabbit BM-MSCs (n=6) became attached to the bottom of the flasks (touchdown) within approximately 2-3 d. Early cell culture revealed spindle shaped cells arranged in colonies. The adherent colonies, observed by inverted phase contrast microscope, in primary culture of BM-MSCs colonies were formed of rounded, yellowish cells at center and some spindle fibroblastoid adherent cells at the periphery (elongated with tapering ends) (Figure 3C). Fibroblastoid cells population grew until culture reaching (80-90%) confluence in flask after 5 d (Figure 3D), at which time that the population was trypsinized and passaged (first passage) (Figure 3E-H). All rabbit BM-MSCs showed growth representing a success rate 100%. On average, first confluence was noticed after 5 d ± 1.00 day from start of culture in expansion medium especially after 2 d from changing medium. The confluence was appeared as fibroblastoid cell population around nodules in different fields of flask and the cell density increased majority of cells exhibited fibroblast-like morphology. Not whole flask was confluence. Nodular confluence was more important than flask confluence. The average yield of viable cells in confluent primary culture of all rabbit BM-MSCs was 0.5-1 x 10^6
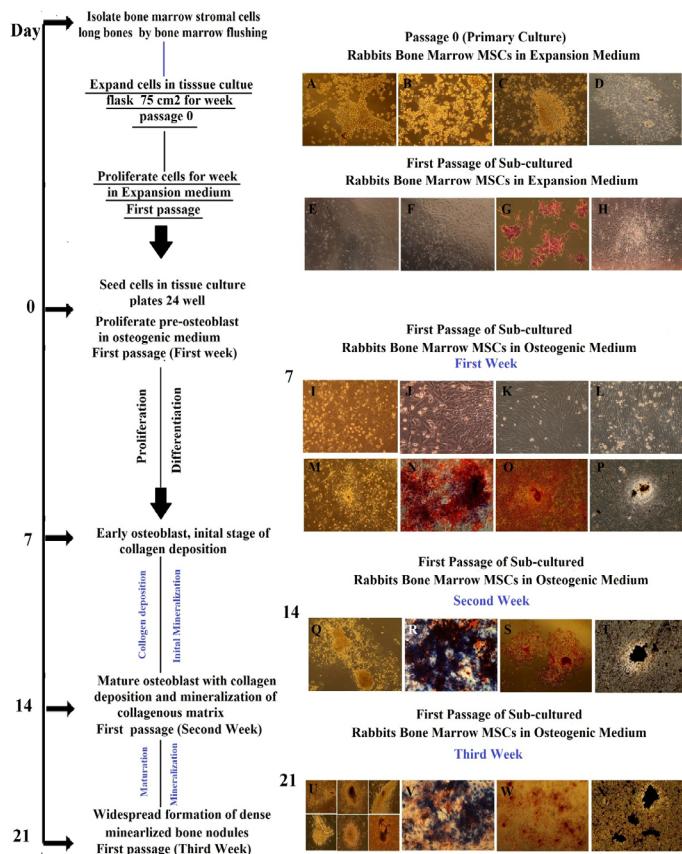
Figure 3: Morphology representation of cultured Rabbit BM-MSCs in expansion medium and their osteogenic differentiation potential with specific markers through first passage/ second and third week cultured in osteogenic medium; Morphology of cultured Rabbit BM-MSCs in expansion medium, passage 0 (primary cell culture). (**A**) at time 0, colonies of cells were seen by inverted phase contrast microscope in expansion medium, Cells were obtained by bone marrow flashing. (**B**) at day 2, elongated cells were appeared and selected by adherence to plastic, whereas floating cells are residual red blood cells and unattached mononuclear cells were maintained in expansion medium. (**C**) at day 3, following removal of non-adherent hematopoietic stem cell populations by changing medium for first time, adherent colonies. The number of colonies varied from 3-7 per flask. Central cells showed high nucleo cytoplamic ratio with little cytoplasm. (**D**) at day 7, fibroblastoid cell population proliferated and increased in density with time and nodular confluence (80-90%) was noticed. Confluence appeared as marked increase in fibroblastoid cell population in colonies (nodules). Morphology of sub-cultured Rabbit BM-MSCs in expansion medium, first passage. (**E, F**) thin and fiberoblast-like MSCs were seen and widespread in all culture plate after trypsinization. (**G**) By hematoxylin and eosin, the cells were polygonal with pink to light violet cytoplasm and blue nucleus. (**H**) Thin and fiberoblast-like MSCs were arranged and expanded in bundles and sheets at day 7 of first passage in expansion medium. Morphology of sub-cultured Rabbit BM-MSCs in osteogenic medium,

first passage through first week of differentiation, alkaline phosphatase histochemical staining, Alizarin Red staining and von Kossa staining. (**I-K**) Rabbit BM-MSCs assumed a less elongated, polygonal, cubodial appearance with central rounded nuclei or multipolar after 48-72 h of subculture. (**L-M**) at day 7 showed coalescing cellular aggregates arranged in swirling sheets and bundles with interconnected multilayer foci showing central matrix-like substance like nodules. (**N**) Osteoblast expressing ALP enzyme were blue interspersed by negative red cells , Positivity of subculture for ALP staining was noticed as early as day 7 with percentage around 20%. (**O**) Orange red color was seen by positive cells in large amount and also, positive cells were interspersed with negative cells. (**P**) Black mineral deposits were seen in large amount and large size. Mineralized areas were interspersed by another un-calcified small cell colony. The characteristic halo, surrounding the bone nodule evidence of the enzymatic activity of the ALP, Inverted Phase Contrast Microscope Digital Camera Olympus, Magnification 10x, Morphology of sub-cultured Rabbit BM-MSCs in osteogenic medium, first passage through second week of differentiation, alkaline phosphatase histochemical staining, Alizarin Red staining and von Kossa staining. (**Q**) The number of nodules increased dramatically in size and becoming multilayered with deposition of collagen and mineralization of collagenous matrix(R) ALP staining was noticed with percentage around 60-80% at day14. (**S**)The mineralized nodules were labeled as red spots with alizarin stain and increased in size dependant on time and number of cells. (**T**) Mineral deposits were stained black with von kossa stain. Morphology of sub-cultured Rabbit BM-MSCs in osteogenic medium, first passage through thrid week of differentiation, alkaline phosphatase histochemical staining, Alizarin Red staining and von Kossa staining. (**U**) The number of nodules increased dramatically in size with widespread formation of dense mineralized bone structure. (**V**) Decline in staining intensity for ALP was noticed with percentage around 60% at day 21. (**W**) The mineralized nodules were labeled as red spots and increased in number and staining intensity in a time dependent manner covering more than 80 % of culture plate. (**X**) Mineral deposits were stained black with von kossa stain and almost of black mineral deposits areas were mostly located in the central confluent multilayered clusters of cells.

IMMUNOPHENOTYPIC CHARACTERIZATION OF MSCS-DERIVED MULTI-POTENT CELLS

Flow cytometric analysis of MSC-derived cells revealed that cells isolated by the described method were negative for CD34; a positive hematopioteic marker and a negative MSCs marker. On the other hand, they were all positive for MSC-specific antigens such as CD90, CD146, CD73 and CD105 (Figures 4 and 5).
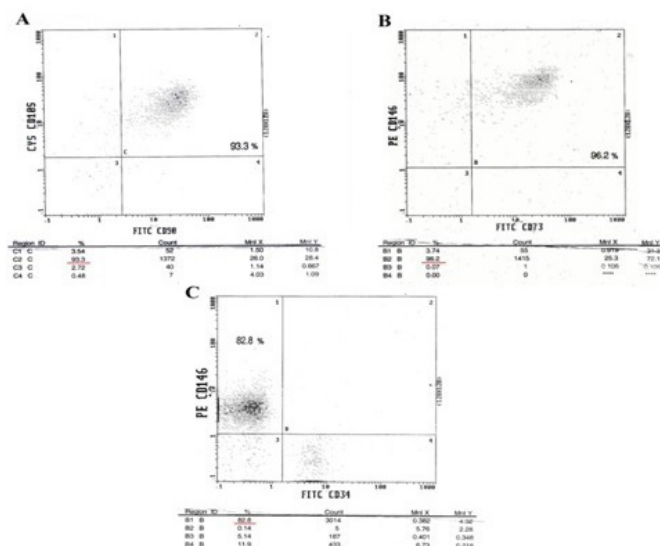
Figure 4: Immuno-phenotype of MSC-derived multipotent cells. Cells were isolated, expanded and analyzed by flow cytometric analysis with antibodies against the indicated antigens of hematopoietic and mesenchymal lineage markers (CD34, CD90, CD146, CD73 and CD 105), the rate positive staining for (A) CD 105 and CD 90 93.3%, (B) CD146 and CD73 96.2% and (C) CD146 82.8%, which confirms their mesenchymal characteristics but negative for CD34.
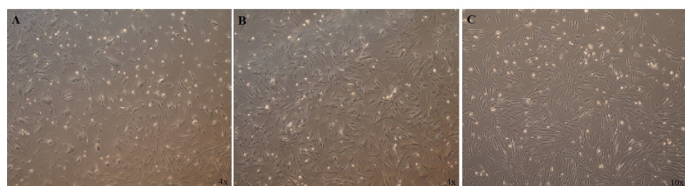

Figure 5: Morphology of MSC-derived multipotent cells by inverted microscope, Cells were isolated by flow cytometric analysis expanded in complete expansion medium (A-C) Condensation of thin and elongated mesenchymal stem cells with morphology of fibroblast through the period of culture and subculture in expansion medium.

OSTEOGENIC DIFFERENTIATION

FIRST PASSAGE (FIRST WEEK, SECOND WEEK AND THIRD WEEK)

The morphology of many cells withtin the population grown in osteogenic medium changed approximately the first 48-72 h following addition of the osteogenic medium. The center of cubodial cells were observed to develop further within BM-MSCs culture. The center of cubodial cells protruding from the monolayer of cell culture (Figure 3I-M). the areas of cellular conglomerates were surrounded by irregulary shaped areas, where cells maintained the spindle cell morphology. Many fields at day 7 showed coalescing cellular aggregates arranged in swirling sheets and bundles with interconnected multilayer foci showing central matrix-like substance like nodules.

Cells formed multilayer structures (nodule structures) where mineralization occurs can be observed. Nodules were formed of two layers; upper layer of cubodial cells and lower layer of presumed extracellular matrix. These nodules increased progressively in size and coalesced to form geographic areas in time dependent manner start with day 7 d to 14 d and 21 d and became mineralized, the late stage of differentiation and function of the osteoblasts.

Table 1: Glass composition in mole %.

	SiO$_2$	CaO	P$_2$O$_5$	CeO$_2$
BG-C0	80	15	5	0
BG-C5	75	15	5	5
BG-C10	70	15	5	10

MINERALIZATION ASSAYS
FIRST PASSAGE (FIRST WEEK, SECOND WEEK AND THIRD WEEK)

Alkaline phosphatase activity assays: The ALP activity qualitatively and quantitatively detected in osteoblast cells at d 7, 14 and 21 was significantly higher in OM-stimulated culture than control ($P > 0.05$). ALP activity was significantly increased from day 0 to day 7, and then significantly decreased progressively till day 21 relative to a peak at day 7. Qualitative ALP histochemical stain confirmed quantitative ALP assay results (Table 2). ALP staining appeared at day 7 and osteoblast expressing ALP enzyme were blue with percentage around (40% - 60%) (Figure 3N) followed by decline in staining intensity for ALP between day 14 and day 21 (Figure 3R and V). Control groups were negative for ALP staining and appeared with red color after 7, 14 and 21 d (Figure 6).

Table 2: Absorbance values (mean ± SD) of alkaline phosphatase enzyme of multipotent stem cells in osteogenic medium and control after 7, 14 and 21 d were measured by ELISA at 405 nm.

Time (day)	Expansion medium	Osteogenic medium
	Control	Osteogensis
7	0.175± 0.013	1.489± 0.028
14	0.165± 0.003	0.892± 0.036
21	0.145± 0.023	0.433± 0.035

The level of ALP enzyme was determined in relation to standard curve. Significantly increase in specific activity of the enzyme in osteogenic subculture of multipotent stem cells compared with control at 7, 14 and 21 d ($P > 0.05$). D= d; n= number.

MATRIX MINERALIZATION ASSAYS
Number of orange red spots with Alizarin Red staining and brown-black mineral deposits with von Kossa staining were seen in the ECM by day 7 of osteogenic induction (Figure 3O and P) and increased in time dependent manner at day 14 (Figure 3S and T) till day 21 (Figure 3W and X). Calcium phosphate was deposited firstly in

the nodular areas then distributed throughout the culture multiwell. Early, mineral deposition was in the form of tiny foci and with time mineralized foci increase in size an coalesce to form bigger areas Orange red colored calcium deposition and brown-black colored phosphate deposition were observed in areas of mineralization by inverted phase contrast microscope and also by naked eye. Control groups were different from osteogenesis groups in their morphology (Figure 6A-R) and were negative for mineralization staining through three weeks of osteogensis process (Figure 6S-U).
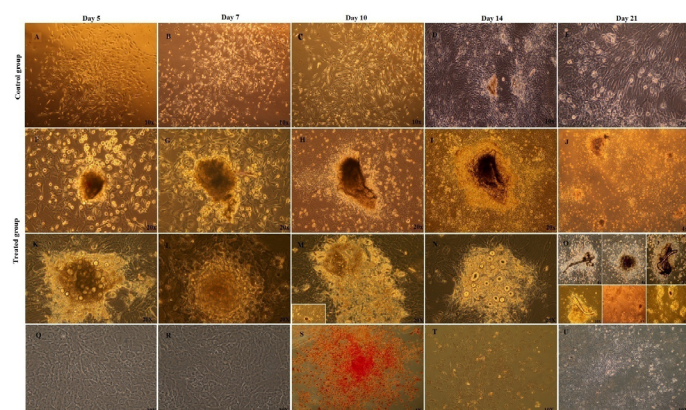

Figure 6: Morphology of MSCs control group subcultured in complete expansion medium and other treated subgroup sub-cultured in osteogenic medium supplemented with b-FGF during three weeks after subculture: (A-E) control group, thin and fiberoblast-like MSCs were arranged in bundles and sheets after subculture at d (A) 5, (B) 7, (C) 10 and (D, E) network pattern of growth was seen. Networks were connected to each other's via long cellular processes at day 14 and 21(F-R) Nodule formation was observed at day 5 in osteogenic medium, and increased in size and number progressively over time during three weeks of subculture. (Q, R) Morphology of MSCs completely different from morphology of osteoblast cells, black arrow,(S) Alkaline phosphatase histochemical staining of control group; the cells were negative for ALP staining (red) at d 7,14, and 21,(T,U) control group was negative for both Alizarin red and Von Kossa staining through three week of differentiation.

EVALUATION OF SCAFFOLDS BIOACTIVITY
A. Direct contact: cells with scaffolds
B. Indirect contact: cells with scaffolds extracts

The cells were stained positively for extracellular mineralization. Mineralization was evident at day 14 (second week) with orange red deposits with (Alizarin Red staining) (Figure 7A-D) and orange red deposits interspersed with black mineral deposits with both (Alizarin and von Kossa staining) together at day 21 (third week) (Figure 6E-H). This demonstrated that all scaffolds were had no observable negative effects on BM-MSCs

osteogenic differentiation. All scaffolds enhanced and maintained cell survival and supported osteogenesis. Also, all scaffolds extract after stained with von Kossa staining, brown-black mineral deposits area were observed to spread in large number of cell colony in different fields of culture plates by inverted microscope (Figure 8) and by naked eye (Figure 9).
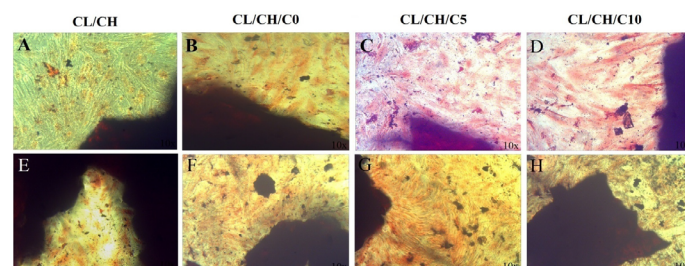

Figure 7: Alizarin Red and von Kossa staining of osteoblastic like-cells of first passage/ second and third week cultured in osteogenic medium with the scaffolds. (A-D) (Second week, orange red color was seen by positive cells in large amount in the vicinity of the scaffold surfaces and stained alizarin red stain at day 14. (E-H) Third week, orange red color was seen by positive cells in large amount interspersed with black mineral deposits with both (Alizarin Red/ von Kossa Staining) together at day 21. Inverted Phase Contrast Microscope Digital Camera Olympus, Magnification 10x.
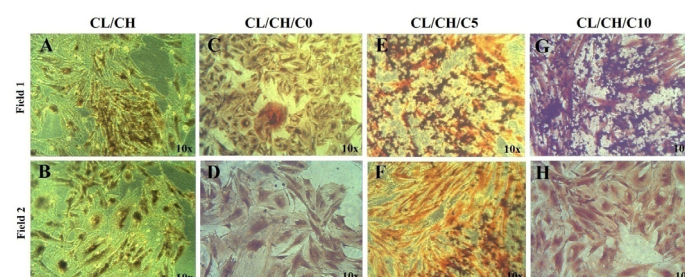

Figure 8: von Kossa staining of osteoblastic cells of first passage/ third week at day 21 cultured in osteogenic medium barrel to cells were seeded with the various of scaffolds extract (A-H) two fields for each scaffold extract brown -black mineral deposits (Mineralized areas) were seen by large cell colony in different fields of culture well, Inverted Phase Contrast Microscope Digital Camera Olympus, Magnification 10x.

CELL VIABILITY ASSAY
Cerium treatment induced a detectable increase in cell growth and proliferation of osteoblast-like cells through first week of differentiation and increased with the treatment time. Cell viability increased beyond that of the cells exposed to scaffold Cl/CH/C10 whereas the cell viability incidence of cells exposed to col/chit alone decreased compared with control. Also, Cell viability proved that all scaffolds and its extracts showed proliferation inhibition through week < 25% reference to final cell number of control group, (zero
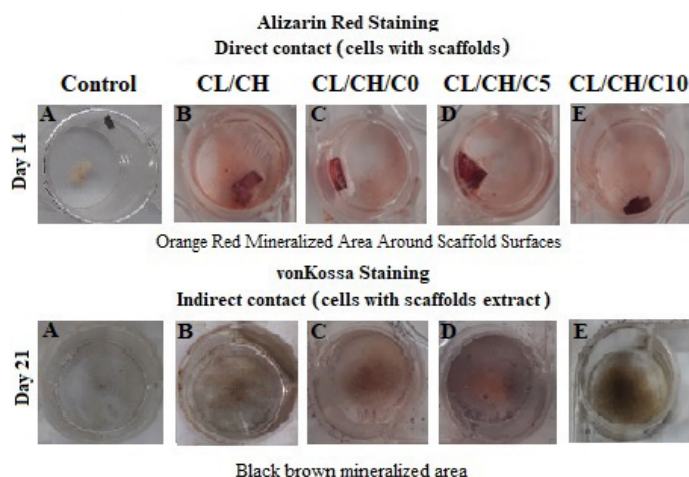
inhibition to proliferation) (Figure 10).

Figure 9: Alizarin Red and von Kossa staining of osteoblastic cells of first passage/ second and third week sub-cultured in osteogenic medium direct and indirect with the scaffolds by naked eye. (A-E) Direct contact at day 14, orange red color was seen by positive cells in large amount in the vicinity of the scaffold surfaces by alizarin red staining. (A-E) Indirect contact at day 21, brown -black mineral deposits (Mineralized areas) were seen by large cell colony in different fields of culture well with scaffolds extract by von Kossa staining.
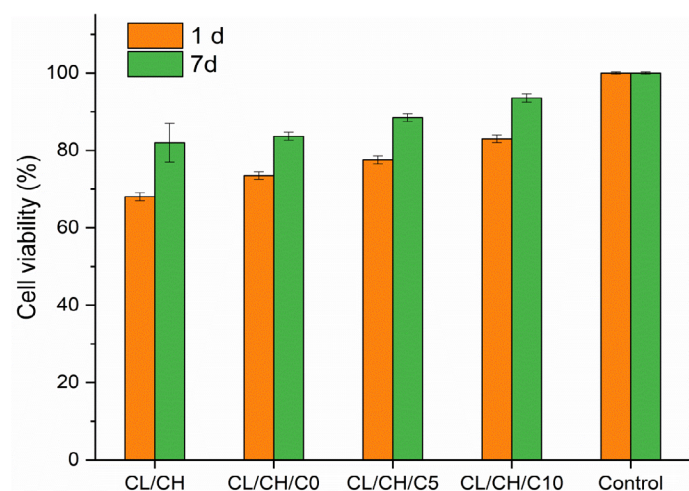

Figure 10: Effect of Cl/CH, Cl/CH/C0, Cl/CH/C5 and Cl/CH/C10 scaffolds evaluated by proliferation of osteoblast cells in osteogenic medium after 1 and 7 d. All scaffolds showed proliferation inhibition < 25% reference to final cell number of control group, (zero inhibition to proliferation).

ANTICANCER ACTIVITY

The data obtained after analysis the results of SRB test, cellular viability following cerium treatment was showed slightly decreased with four different groups after 1h of treatment compared with control, respectively CL/CH (96.16%), CL/CH/C0 (95.92%), CL/CH/C10 (94.97%), CL/CH/C5 (94.13%). After 24h of treatment, significant

viability decrease was observed compared with control cells. Among the composites, having CL/CH/C5 showed the highest cytotoxic effect and reduced survival rate of osteosarcoma cells to 75.68%. The results of cytotoxicity after 1 h and 24 h with and without cerium oxide particles were compatible with cell morphology for all composite materials by inverted microscope. The lowest concentration of CeO_2 reduced survival of osteoarcoma cell line after 24 hr. Also, the subsequent increase of CeO_2 concentration was effective but its effect was less to CeO_2 concentration level 5. Besides, two different concentrations of CeO_2 leads to the increased inactivation of osteosarcoma cells compared with other two composites CL/CH, CL/CH/C0 and control cells. the results showed that all different composite caused cytotoxicity, cell viability at exposure time 24 h decreased to CL/CH (82.43%), CL/CH/C0 (82.09%), CL/CH/C10 (80.94%), CL/CH/C5 (75.68%) respectively and the composite scaffold with low level of concentration 5 was significantly greater than all other groups and caused growth inhibition to osteosarcoma cells more than 24% through one day. Results are qualitatively and quantitatively detected in osteosarcoma cells and expressed relative to control cells (incubated without discs of composites materials) survival rate of control was considered as 100%, the analysis data is shown in (Table 3) and by inverted microscope (Figure 11).
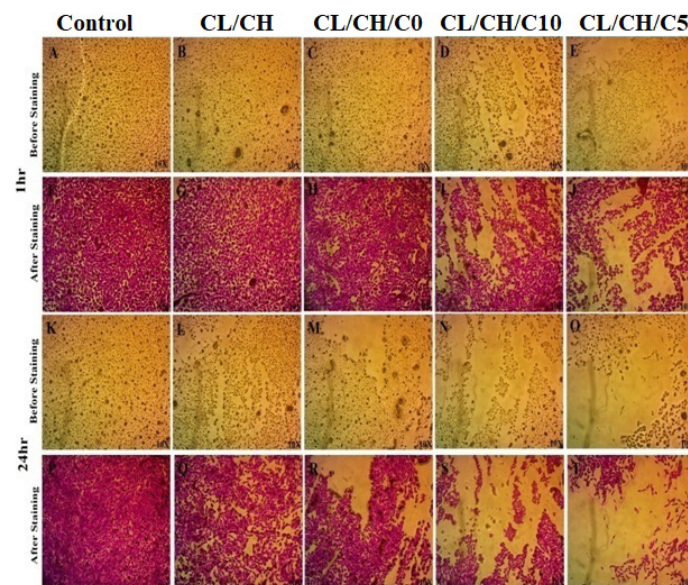

Figure 11: The viability results of the Ce-doped bioactive glass nanoparticles composite scaffolds on osteosarcoma cells. (A-T) The results were shown for Cl/CH, Cl/CH/C0, Cl/CH/C5 and Cl/CH/C10, respectively before and after staining by SRB stain from three independent experiments at exposure time 1h and 24h of treatment. Cell viability decreased respectively and the composite with low level of cerium concentration 5 was significantly greater than all other groups and control cells and caused growth inhibition to osteosarcoma cells more than 24%, Inverted Phase Contrast Microscope Digital Camera Olympus, Magnification 10x.

Table 3: The viability results of the Ce-doped bioactive glass nanoparticles scaffolds on osteosarcoma cells, the results were shown as mean ± SD from three independent experiments at exposure time 1h and 24h of treatment.

Sample	1 h			24 h		
	Mean± STD	Cell viability %	Inhibition %	Mean ± STD	Cell viability %	Inhibition %
CC	0.803±0.006	96.16%	3.84%	0.887±0.02	82.43%	17.57%
BG-C0	0.801±0.003	95.92%	4.08%	0.8833 ±0.02	82.09%	17.91%
BG-C5	0.0786±0.005	94.97%	5.03%	0.81433 ±0.018	75.68%	24.32%
BG-C10	0.793±0.0055	94.13%	5.87%	0.871±0.017	80.94%	19.06%
Control	0.835±0.008	100%	0	1.076±0.131	100%	0

The biocompatibility of the composite scaffolds prepared in this study was evaluated by in vitro non-cellular test in SBF and in vitro cellular test (morphology expression, proliferation and cytotoxicity) against rabbit bone marrow derived mesenchymal stem cells (rBM-MSCs). The in vitro test in SBF was showed that the glass nanoparticles were improved formation of the bone-like apatite layer. This can be explained by the rapid ion exchange between Ca^{2+} and H_3O^+ or H^+ in SBF solution causing a broking of Si-O-Si glass network bonds and formed silica-rich layer composed of silanol (SiOH) groups on the scaffold surfaces. This silica-rich layer owned the affinity to attract Ca^{2+} and PO_4^{3-} from the soaking solution and successively formed bone-like apatite crystals (Kim et al., 1989; Kokubo et al., 1990).

The cells were cultured and incubated in osteogenic media with these scaffolds. The results presented that the composite scaffolds were showed the least toxic effect on the behavior of BM-MSCs which partially directed into osteoblast lineage through only one week of culture in osteogenic media. Moreover, the incorporation of CeO_2 in the glass filler of collagen/chitosan scaffolds was significantly increased the cell viability and proliferation, and the composite scaffold with the highest CeO_2 content (sample Cl/CH/C10) showed the least toxic effect to BM-MSCs. These findings were compatible with the previous study (Karakoti et al., 2010) in which reported that Ce ions enhance proliferation and osteogenic differentiation of the cells and collagen formation by neutralizing oxidative stress which is involved in the development and progression of many diseases.

The determination of hydroxyapatite (HAp) mineralization which is the mineral part of the bone was conducted by the most common mineralization stains (alizarin and von Kossa) The results showed that osteogenically stimulated MSCs were positive for alizarin red (orange red) and von Kossa (brown black) stainings. This finding confirmed presence of hydroxyapatite (this confirmed the in vitro results in SBF) which was more dominant in the scaffold containing the highest percentage of CeO_2 (sample Cl/CH/C10) than the other scaffolds. This can be explained by the phosphatase-mimetic activity of CeO_2 which enhance osteoblastic differentiation of MSCs and collagen formation. The result of this investigation was concordant with the previous study (Karakoti et al., 2010).

The antitumor activity test was revealed that Ce-doped bioactive glass nanocomposite scaffolds was showed a significant toxicity on the osteosarcoma cells after exposure time 24 h comparing to control cells. Moreover, the scaffolds containing glass of low content of CeO_2 was decreased the survival rate of osteosarcoma cells better than that of high CeO_2 content. This means that Ce-doped bioactive glass composite scaffolds having an oxidant effect on cancer cells. Cerium oxide is capable of production the reactive oxygen species (ROS) in acidic pH (tumor cells) by converting the oxidation state from +3 to +4 and scavenging them in normal pH (normal cells) by converting the oxidation state from +4 to +3. (Das et al., 2007). On the other hand, several studies found that nano cerium oxide were able to motivate a significant oxidative stress that could cause the decrease of cell proliferation or even cell death via an apoptoic or necrosis pathway (Higuchi, 2004). However, the cerium oxide toxicity remains controversial and data are still missing to firmly conclude on this issue. This could be explained by the fact that the biological response often depends on several physicochemical parameters; especially pH and cell type.

CONCLISIONS AND RECOMMENDATIONS

The present study showed that using of Ce-doped bioactive glass nanoparticles as filler in collagen/chitosan scaffold was improved formation of bone-like apatite layer on the scaffold surfaces. Moreover, it enhanced the osteoblastic differentiation of MSCs, the highest content cerium was exhibited good biocompatibility and stimulated both the proliferation of BM-MSCs and the osteogenic differentiation of osteoblast cells than that of low content. Furthermore, Ce-doped bioactive glass nanoparticles were enhanced the antitumor activity of the scaffolds, and this activity was higher for the scaffold of low cerium content (sample Cl/CH/C5) than that of high (sample

Cl/CH/C10) on in the scaffold. It may be concluded that collagen/chitosan/Ce-doped nanobioactive glass composite scaffolds can be applied for bone regeneration and anticancer material.

ACKNOWLEDGEMENTS

The authors would like to thank the National Research Centre (Biomaterials Group), National Cancer Institute (Cairo University) and Faculty of Science (Beni-Suef University), Egypt for a possibility to use their facilities.

NOVELTY STATEMENT

It was first time to prepare nanocomposite scaffolds based on Ce-doped bioactive glass nanoparticles, chitosan and collagen natural polymers, and doing detailed biocompatibility for those scaffolds and study the effect of CeO_2 in glass filler on the biocompatibility of the final scaffold with osteoblast cells derived from bone marrow mesenchymal stem cells of rabbit, as well as, study the anticancer activity against MG-63 osteosarcoma cells. The scaffolds contained Ce ions were showed good biocompatibility with the osteoblastic cells, and good anticancer activity.

AUTHOR'S CONTRIBUTION

HFH and MMF wrote the manuscript. MMFEL-D, MAG and BMM conceived the idea. MMF edited the manuscript. All authors have read and approved the manuscript.

ABBREVIATIONS
BM-MSCs: bone marrow mesenchymal stem cells; ROS: reactive oxygen species; MTT: 3-[4,5-dimethythiazol-2-yl]-2,5 diphenyl tetrazolium bromide; BG: Bioglass; NGB: Nanobioactive glasses; CL: Collagen; CH: Chitosan; SEM: Scanning electron microscopy; DMEM: Dulbecco's Modified Eagle Medium; EDX: Energy dispersive X-ray analysis; β-GP: beta- glcerophosphate; ALP: Alkaline phosphatase; b-FGF: basic fibroblast growth factor.

ETHICAL APPROVAL
The study was approved by the Ethics Research Committee of the Faculty of science, Beni-Suef University, Beni-Suef, Egypt (Ethics approval number: 021-194. The study protocol was registered with department of biochemistry as a part of thesis for Ph.D. degree in science.

CONFLICT OF INTEREST

The authors have declared no conflict of interest.

REFERENCES

Abbasi N, Masoud HT, Touran A, Sana R (2021). Cerium oxide nanoparticles-loaded on chitosan for the investigation of anticancer properties. Mater. Technol., pp. 1-11. https://doi.org/10.1080/10667857.2021.1954279

Arima Y, Hiroo I (2007). Effect of wettability and surface functional groups on protein adsorption and cell adhesion using well-defined mixed self-assembled monolayers. Biomaterials, 28: 3074-3082. https://doi.org/10.1016/j.biomaterials.2007.03.013

Arpornmaeklong, Premjit, Maytha S, Komsan A, Supakorn B (2021). Characteristics and biologic effects of thermosensitive quercetin-chitosan/collagen hydrogel on human periodontal ligament stem cells. J. Biomed. Mater. Res. B Appl. Biomater., 109: 1656-1670. https://doi.org/10.1002/jbm.b.34823

Asgharzadeh, Fereshteh, Alireza H, Farzad R, Atieh Y, Seyedeh EN, Amir A, Seyed MHM, Saman S, Majid K (2021). Cerium oxide nanoparticles acts as a novel therapeutic agent for ulcerative colitis through anti-oxidative mechanism. Life Sci.,278: 119500. https://doi.org/10.1016/j.lfs.2021.119500

Augello, A, Cosimo DB (2010). The regulation of differentiation in mesenchymal stem cells. Hum. Gene Ther., 21: 1226-1238. https://doi.org/10.1089/hum.2010.173

Bouzigues C, Thierry G, Antigoni A (2011). Biological applications of rare-earth based nanoparticles. ACS Nano, 5: 8488-8505. https://doi.org/10.1021/nn202378b

Celardo, Ivana, Jens ZP, Enrico T, Lina G (2011). Pharmacological potential of cerium oxide nanoparticles. Nanoscale, 3: 1411-1420. https://doi.org/10.1039/c0nr00875c

Corma A, Pedro A, Hermenegildo G, Jean-Yves C-C (2004). Hierarchically mesostructured doped CeO 2 with potential for solar-cell use. Nat. Mater., 3: 394-397. https://doi.org/10.1038/nmat1129

Das M, Swanand P, Neelima B, Jung-Fong K, Lisa MR, Sudipta S, James JH (2007). Auto-catalytic ceria nanoparticles offer neuroprotection to adult rat spinal cord neurons. Biomaterials, 28: 1918-1925. https://doi.org/10.1016/j.biomaterials.2006.11.036

Declercq H, Natasja VdV, Erna DM, Ronald V, Etienne S, Leo DR, Maria C (2004). Isolation, proliferation and differentiation of osteoblastic cells to study cell/biomaterial interactions: Comparison of different isolation techniques and source. Biomaterials, 25: 757-768. https://doi.org/10.1016/S0142-9612(03)00580-5

Deen, I, Gurpreet SS, Zhiming MW, Federico R (2022). Electrophoretic deposition of collagen/chitosan films with copper-doped phosphate glasses for orthopaedic implants. J. Coll. Inter. Sci., 607: 869-880. https://doi.org/10.1016/j.jcis.2021.08.199

Deliormanlı AM (2015). Synthesis and characterization of cerium and gallium-containing borate bioactive glass scaffolds for bone tissue engineering. J. Mater. Sci. Mater. Med., 26: 67. https://doi.org/10.1007/s10856-014-5368-0

Du J, Leopold K, Jennifer LR, Yongsheng C, Carlo GP, Robert W, James B (2011). Structure of cerium phosphate glasses: molecular dynamics simulation. J. Am. Ceram. Soc., 94: 2393-2401. https://doi.org/10.1111/j.1551-2916.2011.04514.x

Farag MM, Zainab MR, Manar MA (2019). *In vitro* drug release

behavior of Ce-doped nano-bioactive glass carriers under oxidative stress. J. Mater. Sci. Mater. Med., 30: 18. https://doi.org/10.1007/s10856-019-6220-3

Gao K, Xiaoyan W, Zhonghua W, Lijiao H, Jiayu L, Zhenzu B, Kai J, Shan H, Weijia Z, Long L (2021). Design of novel functionalized collagen-chitosan-MBG scaffolds for enhancing osteoblast differentiation in BMSCs. Biomed. Mater., 16: 065028. https://doi.org/10.1088/1748-605X/ac3146

Goh Y-F, Ammar ZA, Muhammad A, Mohammed RAK, Rafaqat H (2014). *In-vitro* characterization of antibacterial bioactive glass containing ceria. Ceram. Int., 40: 729-737. https://doi.org/10.1016/j.ceramint.2013.06.062

Gordon TD, Schloesser L, Humphries DE, Spector M (2004). Effects of the degradation rate of collagen matrices on articular chondrocyte proliferation and biosynthesis in vitro. Tissue Eng., 10: 1287-1295. https://doi.org/10.1089/1076327041887763

Gupta B, Jason BP, Ali MK, Delbert ED, Amy BH (2016). Effects of chemically doped bioactive borate glass on neuron regrowth and regeneration. Ann. Biomed. Eng., 44: 3468-3477. https://doi.org/10.1007/s10439-016-1689-0

Hale LV, Ma YF, Santerre RF (2000). Semi-quantitative fluorescence analysis of calcein binding as a measurement of in vitro mineralization. Calcif. Tissue Int., 67: 80-84. https://doi.org/10.1007/s00223001101

Higuchi Y (2004). Glutathione depletion induced chromosomal DNA fragmentation associated with apoptosis and necrosis. J. Cell. Mol. Med., 8: 455-464. https://doi.org/10.1111/j.1582-4934.2004.tb00470.x

Ignatius A, Blessing H, Astrid L, Carla S, Cornelia N-W, Daniela K, Benedikt F, Lutz C (2005). Tissue engineering of bone: effects of mechanical strain on osteoblastic cells in type I collagen matrices. Biomaterials, 26: 311-318. https://doi.org/10.1016/j.biomaterials.2004.02.045

Jaiswal N, Stephen EH, Arnold IC, Scott PB (1997). Osteogenic differentiation of purified, culture expanded human mesenchymal stem cells in vitro. J. Cell. Biochem., 64: 295-312. https://doi.org/10.1002/(SICI)1097-4644(199702)64:2<295::AID-JCB12>3.0.CO;2-I

Kaczmarek B, Kinga N, Agata O, Olha M, Alina S, Krzysztof Ł, Jithin V, Geetha M, Anna MO (2020). Properties of scaffolds based on chitosan and collagen with bioglass 45S5. IET Nanobiotechnol., 14: 830-832. https://doi.org/10.1049/iet-nbt.2020.0045

Kamal AF, Diah I, Ismail HD, Nurjati CS, Errol UH, Susworo R, Achmad AY, Adang B (2013). Biocompatibility of various hydoxyapatite scaffolds evaluated by proliferation of rat's bone marrow mesenchymal stem cells: An *in vitro* study. Med. J. Indones., 22: 202-208. https://doi.org/10.13181/mji.v22i4.600

Karakoti AS, Olga T, Sheng Y, Peter DL, Molly MS, Julian RJ, Sudipta S (2010). Rare earth oxides as nanoadditives in 3-D nanocomposite scaffolds for bone regeneration. J. Mater. Chem., 20: 8912-8919. https://doi.org/10.1039/c0jm01072c

Kim CY, Arthur EC, Larry LH (1989). Early stages of calcium-phosphate layer formation in bioglasses. J. Non-Cryst. Solids, 113: 195-202. https://doi.org/10.1016/0022-3093(89)90011-2

Kokubo T, Hiroaki T (2006). How useful is SBF in predicting in vivo bone bioactivity? Biomaterials, 27: 2907-2915. https://doi.org/10.1016/j.biomaterials.2006.01.017

Kokubo T, Setsuro I, Huang ZT, Hayashi T, Sakka S, Kitsugi T, Yamamuro T (1990). Ca, P rich layer formed on high strength bioactive glass ceramic A W. J. Biomed. Mater. Res. A., 24: 331-343. https://doi.org/10.1002/jbm.820240306

Lahiji A, Afshin S, David SH, Carmelita GF (2000). Chitosan supports the expression of extracellular matrix proteins in human osteoblasts and chondrocytes. J. Biomed. Mater. Res., 51: 586-595. https://doi.org/10.1002/1097-4636(20000915)51:4<586::AID-JBM6>3.0.CO;2-S

Lehmann G, Paola P, Ilaria C, Raffaella P, Luisa C, Rossella B, Gregorio S, Alessandra B, Antonella C, Laura M (2010). Design, production and biocompatibility of nanostructured porous HAp and Si-HAp ceramics as three-dimensional scaffolds for stem cell culture and differentiation. Ceramics-Silikaty, 54: 90-96.

Leonelli C, Lusvardi G, Malavasi G, Menabue G, Tonelli M (2003). Synthesis and characterization of cerium-doped glasses and *in vitro* evaluation of bioactivity. J. Non-Cryst. Solids, 316: 198-216. https://doi.org/10.1016/S0022-3093(02)01628-9

Li M, Peng S, Can X, Jinsong R, Xiaogang Q (2013). Cerium oxide caged metal chelator: Anti-aggregation and anti-oxidation integrated H2O 2-responsive controlled drug release for potential Alzheimer's disease treatment. Chem. Sci., 4: 2536-2542. https://doi.org/10.1039/c3sc50697e

Lin W, Yue-wern H, Xiao-Dong Z, Yinfa M (2006). Toxicity of cerium oxide nanoparticles in human lung cancer cells. Int. J. Toxicol., 25: 451-457. https://doi.org/10.1080/10915810600959543

Maccarone R, Annamaria T, Maurizio P, Marco C (2020). Ophthalmic applications of cerium oxide nanoparticles. J. Ocular Pharmacol. Therapeut., 36: 376-383. https://doi.org/10.1089/jop.2019.0105

Mandoli C, Francesca P, Stefania P, Giancarlo F, Paolo DN, Silvia L, Enrico T (2010). Stem cell aligned growth induced by CeO2 nanoparticles in PLGA scaffolds with improved bioactivity for regenerative medicine. Adv. Funct. Mater., 20: 1617-1624. https://doi.org/10.1002/adfm.200902363

Ng F., Shayne B, Susie K, Konduru SRS, Lucas C, Uma L, Cleo C, Zheng Y, Mohan CV, Mahendra SR (2008). PDGF, TGF-β, and FGF signaling is important for differentiation and growth of mesenchymal stem cells (MSCs): Transcriptional profiling can identify markers and signaling pathways important in differentiation of MSCs into adipogenic, chondrogenic, and osteogenic lineages. Blood, 112: 295-307. https://doi.org/10.1182/blood-2007-07-103697

Nicolini V, Elena V, Gianluca M, Ledi M, Maria CM, Gigliola L, Alfonso P, Francesco B, Paola L (2016). The effect of composition on structural, thermal, redox and bioactive properties of Ce-containing glasses. Mater. Design, 97: 73-85. https://doi.org/10.1016/j.matdes.2016.02.056

Nicolini V, Gianluca M, Ledi M, Gigliola L, Francesco B, Sergio V, Paola L (2017). Cerium-doped bioactive 45S5 glasses: spectroscopic, redox, bioactivity and biocatalytic properties. J. Mater. Sci., 52: 8845-8857. https://doi.org/10.1007/s10853-017-0867-2

Orellana EA, Andrea LK (2016). Sulforhodamine B (SRB) assay in cell culture to investigate cell proliferation. Bio-protocol, PP. 6. https://doi.org/10.21769/BioProtoc.1984

Perez JM, Atul A, Sudip N, Charalambos K (2008). Synthesis of biocompatible dextran coated nanoceria with pH dependent antioxidant properties. Small, 4: 552-556.

https://doi.org/10.1002/smll.200700824

Placek LM, Keenan TJ, Coughlan A, Wren AW (2018). Investigating the effect of glass ion release on the cytocompatibility, antibacterial efficacy and antioxidant activity of Y2O3/CeO2 doped SiO2-SrO-Na2O glasses. Biomed. Glasses, 4: 32-44. https://doi.org/10.1515/bglass-2018-0004

Rao LG, Liu LJ-F, Timothy MM, Elizabeth M (2001). 17β-estradiol stimulates mineralized bone nodule formation when added intermittently to SaOS-2 cells. Drug Metab. Drug Interact., 18: 149-158. https://doi.org/10.1515/DMDI.2001.18.2.149

Rinaudo M (2006). Chitin and chitosan: Properties and applications. Prog. Polymer Sci., 31: 603-632. https://doi.org/10.1016/j.progpolymsci.2006.06.001

Shruti S, Antonio JS, Gianluca M, Gigliola L, Ledi M, Chiara F, Piercarlo M, Maria V-R (2012). Structural and *in vitro* study of cerium, gallium and zinc containing sol–gel bioactive glasses. J. Mater. Chem., 22: 13698-13706. https://doi.org/10.1039/c2jm31767b

Skehan P, Ritsa S, Dominic S, Anne M, James M, David V, Jonathan TW, Heidi B, Susan K, Michael RB (1990). New colorimetric cytotoxicity assay for anticancer-drug screening. J. Natl. Cancer Inst., 82: 1107-1112. https://doi.org/10.1093/jnci/82.13.1107

Sundararajan V, Devanand GV, Sahabudeen SM (2021). Investigation of therapeutic potential of cerium oxide nanoparticles in Alzheimer's disease using transgenic Drosophila. 3 Biotech., 11: 1-11. https://doi.org/10.1007/s13205-021-02706-x

Suo H, Jiaying Z, Mingen X, Ling W (2021). Low-temperature 3D printing of collagen and chitosan composite for tissue engineering. Mater. Sci. Eng. C, 123: 111963. https://doi.org/10.1016/j.msec.2021.111963

Vichai V, Kanyawim K (2006). Sulforhodamine B colorimetric assay for cytotoxicity screening. Nature Protocols, 1: 1112-1116. https://doi.org/10.1038/nprot.2006.179

Xia W, Jiang C (2007). Preparation and characterization of nano-bioactive-glasses (NBG) by a quick alkali-mediated sol–gel method. Mater. Lett., 61: 3251-3253. https://doi.org/10.1016/j.matlet.2006.11.048

Xu C, Xiaogang Q (2014). Cerium oxide nanoparticle: A remarkably versatile rare earth nanomaterial for biological applications. NPG Asia Mater., 6: e90-e90. https://doi.org/10.1038/am.2013.88

Xu C, Youhui L, Jiasi W, Li W, Weili W, Jinsong R, Xiaogang Q (2013). Nanoceria triggered synergetic drug release based on CeO2 capped mesoporous silica host–guest interactions and switchable enzymatic activity and cellular effects of CeO2. Adv. Healthc. Mater., 2: 1591-1599. https://doi.org/10.1002/adhm.201200464

Yang Y, Alastair CR, Nicola ME (2021). Recombinant human collagen/chitosan-based soft hydrogels as biomaterials for soft tissue engineering. Mater. Sci. Eng. C, 121: 111846. https://doi.org/10.1016/j.msec.2020.111846

Zhang J, Cuilian L, Yaping L, Jing S, Peng W, Keqian D, Yanyan Z (2010). Effect of cerium ion on the proliferation, differentiation and mineralization function of primary mouse osteoblasts *in vitro*. J. Rare Earths, 28: 138-142. https://doi.org/10.1016/S1002-0721(09)60067-3